



HAL
open science

LASER-DIFFRACTION MEASUREMENT OF NONSPHERICAL DROP SPRAYS

Christophe Dumouchel, Jean-Bernard Blaisot

► **To cite this version:**

Christophe Dumouchel, Jean-Bernard Blaisot. LASER-DIFFRACTION MEASUREMENT OF NON-SPHERICAL DROP SPRAYS. *Atomization and Sprays*, 2014, 24 (3), pp.223-249. 10.1615/Atom-izSpr.2014008570 . hal-04663697

HAL Id: hal-04663697

<https://hal.science/hal-04663697v1>

Submitted on 29 Jul 2024

HAL is a multi-disciplinary open access archive for the deposit and dissemination of scientific research documents, whether they are published or not. The documents may come from teaching and research institutions in France or abroad, or from public or private research centers.

L'archive ouverte pluridisciplinaire **HAL**, est destinée au dépôt et à la diffusion de documents scientifiques de niveau recherche, publiés ou non, émanant des établissements d'enseignement et de recherche français ou étrangers, des laboratoires publics ou privés.

LASER-DIFFRACTION MEASUREMENT OF NONSPHERICAL DROP SPRAYS

Christophe Dumouchel & Jean-Bernard Blaisot*

CNRS UMR 6614—CORIA, Université et INSA de Rouen, B.P. 12, 76801 Saint Etienne du Rouvray, France

*Address all correspondence to Christophe Dumouchel
E-mail: christophe.dumouchel@coria.fr

Original Manuscript Submitted: 08/21/2013; Final Draft Received: 12/13/2013

The objective of the present experimental and analytical investigation is to acquire a better understanding and appreciation of the volume-based drop-diameter distribution measured by laser-diffraction technique (LDT) when probing sprays with a significant rate of nonspherical drops. Experiments are performed on sprays of several liquids with a LDT and an image analyzing technique (IAT). IAT is used to attest to and quantify the average nonsphericity of the drops. The LDT diameter distribution characterizes an equivalent system of spherical drops that would produce the same forward light scattered pattern as the one recorded. By modeling this distribution with a three-parameter generalized gamma function according to a recent optimization procedure, it is demonstrated that drop shape influences the fractal characteristic of the LDT distribution in the small diameter region. This suggests that LDT analyzes deformed drops as clusters of smaller drops. Thus, the small drop population of the LDT equivalent system contains information of the actual small drop population and on the shape of the actual drops. The presence of deformed drops manifest by an extended tail of the LDT distribution in the large diameter region also, which results in specific mean diameter series as suspected in previous investigations.

KEY WORDS: *liquid sprays, drop morphology, generalized gamma function, image analysis drop sizing, laser diffraction drop sizing*

1. INTRODUCTION

In many industrial applications, liquids are used under the form of a stream of droplets called a spray. The most common way to produce a spray is to throw out a liquid flow in a gaseous environment. In the absence of the stabilizing effects of walls, the flow is deformed by growing perturbations and disintegrates into liquid drops whose distributions in size, velocity, and shape depend on the injection conditions and influence the efficiency of the application the spray is involved in. Drop size and velocity distributions are often accounted to characterize liquid sprays but this is far less the case of the drop shape. Primary and secondary atomization processes generate nonspherical drops (Ghaemi et al., 2009) and the probability of finding nonspherical drops is high near the

region of spray production. This probability increases with the width of the size and velocity distributions since the drop shape is related to its gaseous Weber number We_G ($= \rho_G V^2 D / \sigma$, where ρ_G is the surrounding gas density, V the drop velocity, D its diameter, and σ the surface tension) (Loth, 2008): the greater this number, the less spherical the drop is. The interaction of drops with the surrounding phase or with each other may also result in the generation of nonspherical drops (Ghaemi et al., 2009). It has been also demonstrated that the interaction between a drop and the continuous gaseous phase and its propensity to breakup are both functions of its initial shape (Black and McQuay, 2001). Drop shapes might have a direct impact on the application. This is the case for instance in combustion mixture process, if evaporation takes place before all drops have reached their asymptotic spherical shape since evaporation depends on the liquid–gas interface area. Thus, as pointed out by Ghaemi et al. (2009), quantification of drop shape in a spray can elucidate several characteristics and mechanisms of the atomization process such as drop production, deformation, breakup, and collision. Furthermore, providing information on the drop shape participates in a more complete characterization of liquid sprays. Experimental and mathematical characterization of sprays containing nonspherical droplets is the investigation field of this work.

The question of drop shape characterization has aroused numerous investigations based on image analysis that is now seen as a competitive approach thanks to recent improvements of computers, camera sensors, and processing techniques. Although imaging techniques provide a two-dimensional (2D) image of a three-dimensional (3D) phenomenon, they allow approaching information in the drop shape. For this purpose, most investigations based on image analyzing technique (IAT) use shape parameters. Ghaemi et al. (2009) have listed no less than 17 shape parameters without counting their possible declinations. Shape parameters indicate a deviation from a reference shape which often is a circle or an ellipse. Focusing their investigation on liquid drops, Ghaemi et al. (2009) identified three main groups of shapes, i.e., spheres, deformed drops, and ligaments, and noticed that most of the shape parameters had difficulties in distinguishing these shapes. They defined a new shape parameter based on the particle concavity or convexity that affects a sign to the traditional shape parameter and allows distinguishing the three shape groups.

Other investigations tackle the question of the measurement of nonspherical particles by using complementary information provided by several diagnostics. Barreiros et al. (1996) used a Coulter Multisizer, a SediGraph instrument, a LDT, and an IAT to analyze three sets of solid particles with known shapes. They found that the diagnostics report different distributions when the particles are not spherical, and concluded from LDT and IAT comparisons that the identification of the LDT diameter with the projected area diameter, i.e., diameter of the circle that has the same surface area as the 2D projection of the particle, is questionable. They also noticed that calculating a mean shape parameter from the diameter distribution reported diagnostic-dependent results and is therefore not recommended. Endoh et al. (1998) analyzed samples of solid particles with a

sedimentation technique and LDT. That work demonstrated a possible relationship between LDT mean diameters and particle shapes as well as the possibility of estimating a mean shape parameter by the ratio of the median diameters determined by LDT and sedimentation. Guardiani et al. (2002) analyzed solid particle samples of known sizes and shapes with IAT and LDT. In agreement with Barreiros et al. (1996), they noticed that the diagnostics reported different diameter distributions for nonspherical samples. They established a Neural Networks model to be applied to the light scattering data in order that LDT reports the same diameter distribution as the one provided by IAT that was considered the reference distribution. Considering that both diagnostics report diameter distributions when nonspherical elements are sampled, this information must be seen as an equivalent-diameter distribution (Black et al., 1996) and none of them is *a priori* a better characteristic than the other. Thus, the choice made by Guardiani et al. (2002) is subject to discussion. The question of drop shape in liquid sprays was approached in a previous experimental work that made use of LDT and IAT (Dumouchel et al., 2010). In that investigation, IAT was not applied to determine individual drop shape parameter but to measure the surface-based scale distribution of the whole spray. Being sensitive to the amount of interface per unit liquid surface area, this distribution is a global multiscale characteristic that is a function of the drop shapes. Correlations between characteristics of LDT distributions and scale distributions were identified, which revealed that LDT distributions contain qualitative information on spray drop morphology.

The present experimental work intends to contribute to a better understanding of the LDT diameter distributions when nonspherical drop sprays are probed. As all laser-based methods, LDT determines the diameter distribution of the equivalent system of spherical drops but the relationship between this equivalent system and the shape of the *actual* drops is difficult to establish (Black et al., 1996). By definition, this equivalent system of spherical drops is the one that produces the same forward light scattered pattern as the one recorded. The work uses the complementarity offered by LDT and IAT measurements. Both diagnostics perform a spatial sampling of the spray and do not segregate drops according to their shape. One of the novel aspects of this investigation concerns a tomographic spray sampling procedure adopted for IAT that allows probing the spray in the same way as LDT. Furthermore, in order to interpret the experimental observations, the LDT distributions are modeled according to a protocol recently established (Dumouchel et al., 2012a,b).

2. EXPERIMENTAL WORK

2.1 Experimental Setup and Operating Conditions

The experimental setup is conceived to produce liquid sprays at low injection pressures under atmospheric conditions of temperature and pressure. The liquid is kept in a pressurized tank and filtered before reaching the injector. The injection pressure ΔP_i is

measured just upstream the injector. A single injector is used. It has a triple-disk nozzle as schematized in Fig. 1(a). [The full description of the nozzle can be found elsewhere (Inj. 2 in Dumouchel et al., 2010).] The single cylindrical discharge orifice in disk 3 has a diameter d_{or} equal to 400 μm and an eccentricity equal to 450 μm . The liquid flow issuing from this injector is a 2D liquid sheet as shown in Fig. 1(b) (water, $\Delta P_i = 0.40$ MPa). The interfaces of the sheet are subject to growing perturbations that constrain the liquid system to reorganize as a ligament network whose disintegration produces liquid drops.

Three liquids are used: water and two water–ethanol mixtures. Their physical properties are given in Table 1 as well as the corresponding Ohnesorge number $\text{Oh} [= \mu_L / (\rho_L d_{or} \sigma)^{0.5}]$ and characteristic capillary time $t_\sigma [= (\rho_L d_{or}^3 / \sigma)^{0.5}]$. The injection pressure is varied as indicated in Table 2 and injections are steady. For every operating condition, the mass flux is measured by weighting the liquid mass collected during a controlled time interval and an average velocity V_q is deduced from this measurement. The Reynolds number $\text{Re} (= \rho_L V_q d_{or} / \mu_L)$ and the gaseous Weber number $\text{We}_G (= \rho_G V_q^2 d_{or} / \sigma)$ that characterize the flow issuing from the nozzle are given in Table 2. The high Reynolds numbers express the role of liquid turbulence in the liquid sheet initial perturbation, whereas the low gaseous Weber numbers are representative of

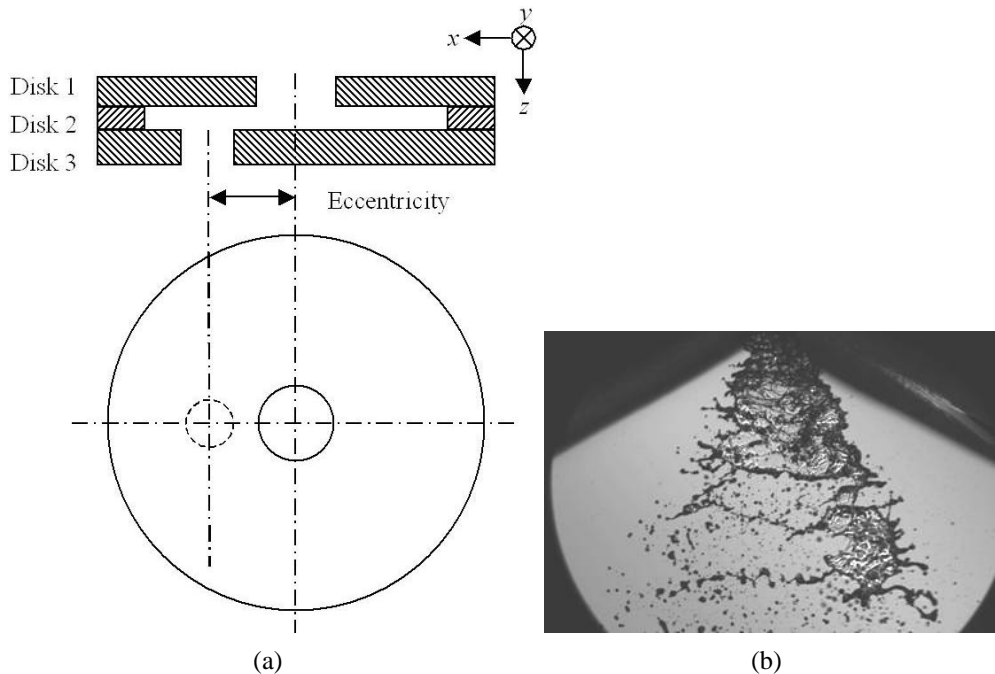


FIG. 1: (a) Injector triple-disk nozzle (side view and top view); (b) Visualization of the issuing liquid flow (water, $\Delta P_i = 0.4$ MPa, 10 mm \times 7 mm).

TABLE 1: Physical properties of the liquids (percentage indicates a proportion in weight), Ohnesorge number Oh , and capillary characteristic time t_σ

Liquid	Density ρ_L (kg/m ³)	Surface tension σ (N/m)	Dynamic viscosity μ_L (kg/ms)	Oh (-)	t_σ (ms)
Water	994	0.070	1×10^{-3}	0.006	0.955
Water-ethanol 10%	973	0.044	1.32×10^{-3}	0.010	1.19
Water-ethanol 15%	967	0.038	1.57×10^{-3}	0.013	1.28

TABLE 2: Injection pressure interval and corresponding ranges of Reynolds and gaseous Weber numbers for all working conditions

Liquid	Injection pressure ΔP_i (MPa)	Reynolds number Re (-)	Gaseous Weber number We_G (-)
Water	0.2–1.0	3800–9000	0.63–3.55
Water-ethanol 10%	0.2–0.6	2720–5220	0.93–3.43
Water-ethanol 15%	0.2–0.6	2300–4290	1.12–3.90

atomization processes free of aerodynamic effect and dominated by surface tension forces (Dumouchel et al., 2005).

In the presentation of the results and analysis, every working condition is associated with the time ratio $\tau = t_e/t_\sigma$, where t_e is a convective time $t_e = h/V_q$ (h being the distance between the nozzle exit section and the position at which the measurement is performed) and t_σ is the capillary time given in Table 1. This ratio can be expressed as a function of the Reynolds and Ohnesorge numbers or of the liquid Weber number ($We_L = \rho_L V_q^2 d_{or}/\sigma$), i.e.,

$$\tau = \frac{t_e}{t_\sigma} = \frac{h}{d_{or} Oh Re} = \frac{h}{d_{or} \sqrt{We_L}} \quad (1)$$

This number can be seen as a corrected liquid Weber number that accounts for the position of characterization. It situates the measurement time in comparison with a physical characteristic time: a small τ characterizes a spray close to the production region (small distance h) or produced at a great injection pressure (high Re number).

The test bench is equipped with two diagnostics mounted on perpendicular optical axis, i.e., the LDT and the IAT. These techniques are never simultaneously used since the spray is not axisymmetric. The injector is always orientated so that the optical axis of the diagnostic used is perpendicular to the liquid sheet, i.e., to the plane of the image shown in Fig. 1(b).

2.2 LDT

The LDT equipment used is the Spraytec 1997 from Malvern. The optical probe is a cylindrical laser beam with a wavelength equal to 670 nm and a diameter equal to 10

mm and the software part of the instrument is based on the Lorentz–Mie theory. The Spraytec is equipped with a 450 mm focal length collecting lens and a detector with 32 diodes. The independent model is selected for the inversion procedure that calculates the volume-based diameter distribution $f_3(D)$ from the recorded forward light scattered pattern. The parameters of this procedure are selected to avoid nonphysical cut in the small drop-diameter population. The adjustable sampling frequency of the instrument is set to 10 Hz and diameter distributions obtained over a 5 s acquisition duration are averaged.

The tuning of the instrument and the measurement procedure are tested with a calibrated reticle containing a series of opaque circles with diameters distributed according to a Rosin–Rammler diameter distribution, i.e.,

$$f_3(D) = q_{RR} \frac{D^{q_{RR}-1}}{D_{RR}^{q_{RR}}} \exp\left(-\left(\frac{D}{D_{RR}}\right)^{q_{RR}}\right) \quad (2)$$

with $q_{RR} = 3$ and $D_{RR} = 50 \mu\text{m}$. Figure 2 shows that the measured diameter distribution agrees well with the expected one and that the agreement sustains a $\log \times \log$ representation. This test also underlines that drops with a diameter as small as $8 \mu\text{m}$ are well measured with the LDT.

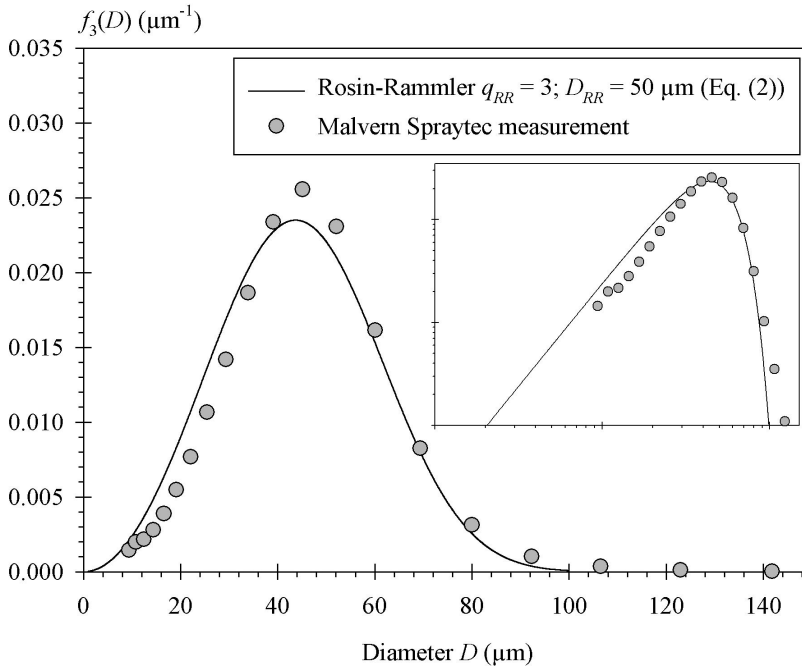


FIG. 2: Volume-based diameter distribution of the set of circles on the reticle. Comparison between the LDT distribution and the expected distribution (Detail: \log – \log representation).

The center of the laser beam was positioned where the probability of finding nonspherical drops was high. However, for every working condition, the atomization process should be completed enough at the measurement location. Using snapshot images, the best distances from the nozzle exit to position the laser beam center were found equal to $h = 12$ mm and $h = 15$ mm for water and the water–ethanol mixtures, respectively. The transmission of the measurements, which is defined by the ratio of the nondeviated light intensity to the incident light intensity, is never less than 75%, which is high enough to exclude any multiple scattering effects. The optional multiple-scattering algorithm of the instrument is therefore not selected.

LDT does not segregate drops according to their shape: all drops, whatever their shapes, passing through the measuring volume are accounted. In this case, the LDT volume-based diameter distribution characterizes the set of spherical drops that would produce the same forward light scattered pattern as the one recorded. According to Sowa (1992), the arithmetic mean of this distribution is equal to the mean diameter D_{43} and its variance is equal to $D_{53}^2 - D_{43}^2$. The ratio variance/(mean)² compares the width of the distribution with its mean and is an indicator of the degree of dispersion of the distribution. This ratio is called the relative dispersion and is noted Δ_3 for the volume-based diameter distribution, i.e.,

$$\Delta_3 = \frac{D_{53}^2}{D_{43}^2} - 1 \quad (3)$$

2.3 IAT

Snapshots of the sprays are performed using a shadowgraph optical arrangement. The light source is a Nanolite from HSPS with a flash duration equal to 20 ns. In the present configuration, this light source plays the role of the shutter. The high-resolution charge-coupled device (CCD) camera is a DALSA Pantera 11M4 (4016×2672 pixels). The physical field covered by the image is equal to 10.5 mm \times 7.0 mm and corresponds to a spatial resolution equal to 2.6 $\mu\text{m}/\text{pixel}$. Reproducing the LDT arrangement, the center of the image is located at $h = 12$ mm (for water) or $h = 15$ mm (for the water–ethanol mixtures) from the injector exit section.

By definition, LDT and IAT measurement volumes are not equal. Imposed by the depth of field, the IAT measurement volume depth is far less than the LDT measurement volume depth since LDT is a line-of-sight technique that performs a spatially integrated sampling. This problem is overcome by applying the tomographic sampling procedure detailed in Dumouchel et al. (2012b). The IAT measurement volume depth is determined by the calibration of the point spread function (Fdida and Blaisot, 2010). For the present optical arrangement, this depth is found equal to 500 μm . An analysis of the size, contrast, and gray level gradient of any drop in the image indicates whether this drop belongs to the measurement volume and should be taken into account. All spray regions are probed by IAT by translating the spray along the optical axis with a step

equal to the measurement volume depth. At every position of the focal plane, a slice of the spray is analyzed and provides local information and all local information is cumulated to reconstruct a whole spray characteristic (see Dumouchel et al., 2012b). Applied to water sprays produced by the present triple-disk injector, this tomographic sampling procedure revealed that the size distribution of the droplets contained in the central region, i.e., when the focal plane contains the discharge orifice axis, is equal to the whole spray size distribution (Dumouchel et al. 2012b). Tests with the two other liquids performed within the scope of the present work report the same behavior. In consequence, IAT measurement and analysis are performed for the central spray region only. As an illustration of this procedure, Fig. 3(a) shows a typical raw image taken when the focal plane contains the discharge orifice axis (water, $\Delta P_i = 0.6$ MPa) and Fig. 3(b) shows the drops that actually belong to the central region of $500 \mu\text{m}$ thickness and that are considered in the analysis. After the identification of the drops belonging to the measurement volume, their respective contour using a subpixel detection procedure is detected and their equivalent diameter and shape parameters are measured. The protocol followed for the image treatment, drop detection, and measurement is the one developed by Fdida and Blaisot (2010).

Equivalent diameter D' and shape parameters Sp and η are individual drop characteristics defined by

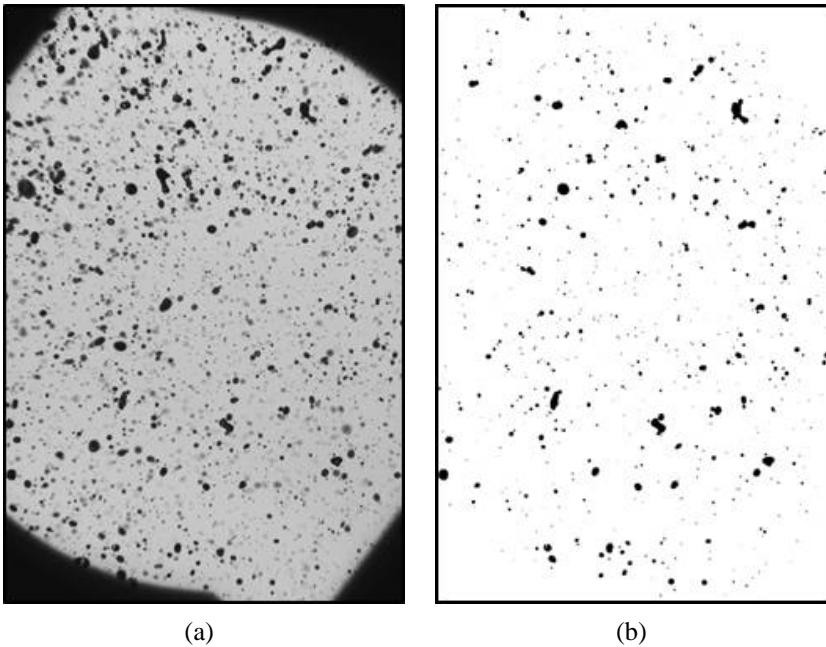


FIG. 3: Image of water spray at $\Delta P_i = 0.6$ MPa. (a) Raw image; (b) drops belonging to the $500 \mu\text{m}$ thick measurement volume.

$$\left\{ \begin{array}{l} D' = \sqrt{\frac{A(S)}{\pi}} \\ Sp = \frac{A(S \cup S_c) - A(S \cap S_c)}{A(S)} \\ \eta = \frac{2(r_{\max} - r_{\min})}{D'} \end{array} \right. \quad (4)$$

The surfaces S and S_c as well as the distances r_{\max} and r_{\min} are shown in Fig. 4 and $A(x)$ designates the area of surface x . In Fig. 4(a), $A(S) = A(S_c)$ and the circle S_c has the same center of gravity as the actual object 2D projection S . $A(S \cup S_c) - A(S \cap S_c)$ is the gray surface area in Fig. 4(a).

In the literature, the equivalent diameter D' is often called the projected area diameter (Black et al., 1996). In the present configuration, the smallest equivalent diameter measured with a sufficient accuracy is equal to 10 μm . Considering all operating conditions, the gaseous Weber number of drops with an equivalent diameter D' less than or equal to 50 μm is never found greater than 0.5. According to the literature (Loth, 2008) these drops are spherical and we may conclude that their IAT equivalent diameter D' is a good measurement of their actual diameter. Thus, we conclude that IAT provides a reliable measurement of the *actual* population of drops with a diameter less than 50 μm .

The shape parameters Sp and η are the sphericity and uniformity, respectively (Blaisot and Yon, 2005). They are both equal to 0 for circular objects and their maximum values are $Sp = 2$ and $\eta \rightarrow \infty$. The shape parameters are measured for drops whose equivalent diameter D' is greater than 50 μm . As an illustration, examples of drops detected on images and their respective value of equivalent diameter and shape parameters measured by IAT are shown in Table 3. In the following, averages of the shape parameters are presented only. These averages are indicators of a mean deviation from circularity of the *actual* spray drops.

For every operating condition, at least 40 images are taken and analyzed and a minimum of 5500 drops are measured. This was found to be sufficient to provide statistical information. The equivalent diameters are dispatched in the same diameter-class series

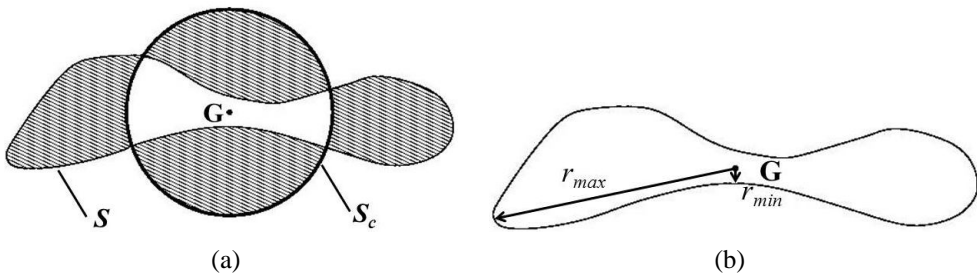











FIG. 4: Definition of the shape parameters. (a) The sphericity parameter; (b) the uniformity parameter.

TABLE 3: Images of drops with their respective equivalent diameter and shape parameters introduced by Eq. (4) and measured by IAT (The images are not to scale)

	D' (μm)	Sp (-)	η (-)
	193	0.04	0.08
	286	0.09	0.22
	302	0.30	0.69
	508	0.50	1.14
	238	0.85	1.74
	648	0.87	1.88
	322	1.06	2.28
	345	1.19	2.17
	400	1.32	2.45

as the one of the LDT and a surface-based equivalent diameter distribution $f_2(D)$ is built.

3. RESULTS AND ANALYSIS

3.1 Drop Shape and LDT Drop-Size Distribution

The first result to be presented concerns the average shape parameters that quantify the average deviation from sphericity of the spray drops. For every working condition, these

parameters are shown in Fig. 5 as a function of the number τ [see Eq. (1)]. The average shape parameters are never equal to 0, which indicates that, on average, drops show a measurable deviation from sphericity. This deviation increases when τ decreases, which makes sense. Indeed, small τ is representative of a measurement performed near the region of drop production or at a great injection pressure. In both situations, the drops have less time to get spherical than if they were measured farther from the production region or if they were produced at a smaller injection pressure. We note that the shape parameters depend on the liquid properties. Indeed, the water–ethanol mixtures, which have the smallest surface tension, report greater shape parameters than water. However, the rate of variation of the average shape parameters with τ is almost independent of the liquid physical properties. In the future, it would be interesting to check whether this behavior agrees with variation of the distance from the nozzle. This observation underlines the appropriateness of the time ratio τ to categorize the present experimental conditions.

LDT measurements are therefore performed on sprays of drops that are nonspherical (on average) and whose average deviation from sphericity depends on the working conditions. Typical equivalent-diameter volume-based distributions obtained in this condition are plotted in Fig. 6 (water, all injection pressure). The distributions show the traditional bell shape characterized by a peak and a modal diameter, i.e., the diameter for which

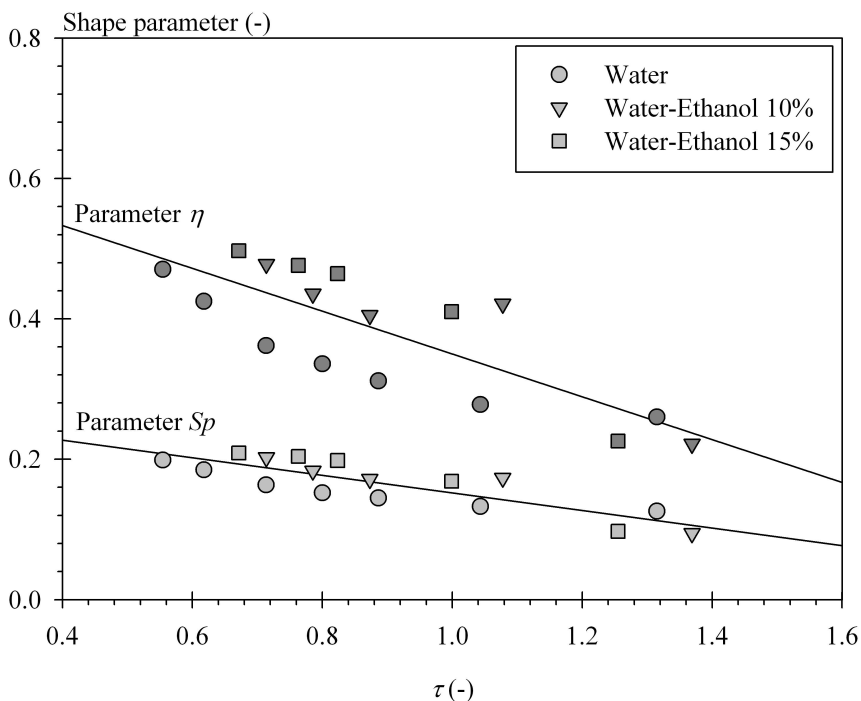


FIG. 5: Average shape parameters versus the number τ .

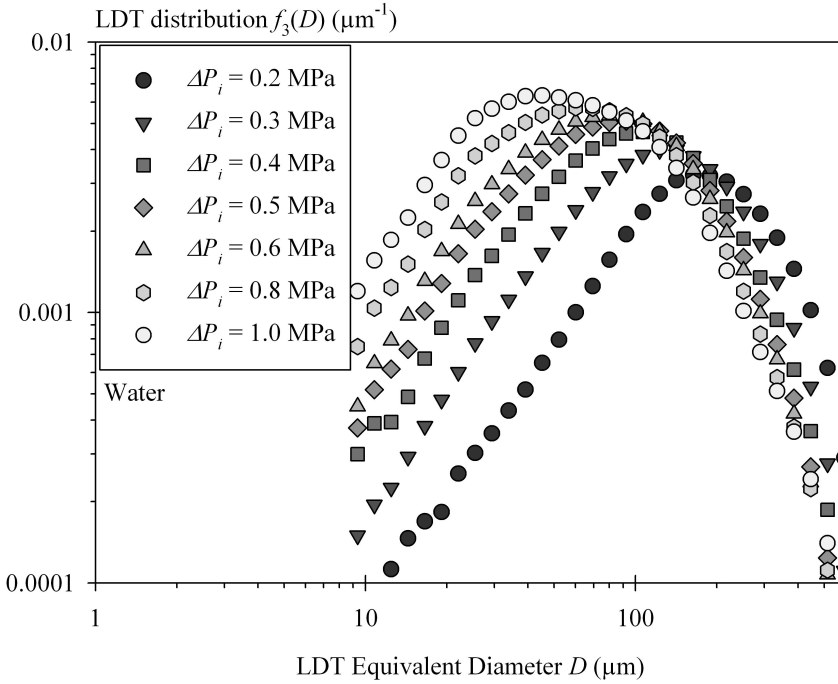


FIG. 6: LDT volume-based diameter distributions (water, influence of the injection pressure).

the distribution is maximum. When the injection pressure increases, the distribution is left shifted (the modal diameter decreases) and the distribution peak increases. Similarly observed for the other liquids, these behaviors are often reported in the literature. The relative dispersion Δ_3 [Eq. (3)] obtained for every working condition is shown in Fig. 7 as a function of τ . This figure evidences an increase of the relative dispersion when τ decreases. Thus, the results in Figs. 6 and 7 say that increasing the injection pressure reduces the drop LDT equivalent diameter but augments the poly-dispersion of the LDT distribution.

Figure 7 shows that the organization of the relative dispersion with τ is rather independent of the liquid. This underlines a sort of universal status of the characteristics τ and Δ_3 when the atomization process remains unchanged over the whole working condition domain as is the case in the present work. Considering that the number τ is a corrected version of the liquid Weber number [Eq. (1)], the strong correlation in Fig. 7 reminds us of the dominance of the surface tension forces in the present disintegration process.

The influence of the drop shape on the LDT equivalent-diameter distribution can be shown by comparing LDT and IAT distributions. Indeed, these two diagnostics report equal-diameter distribution if and only if all drops are spherical. Otherwise, as

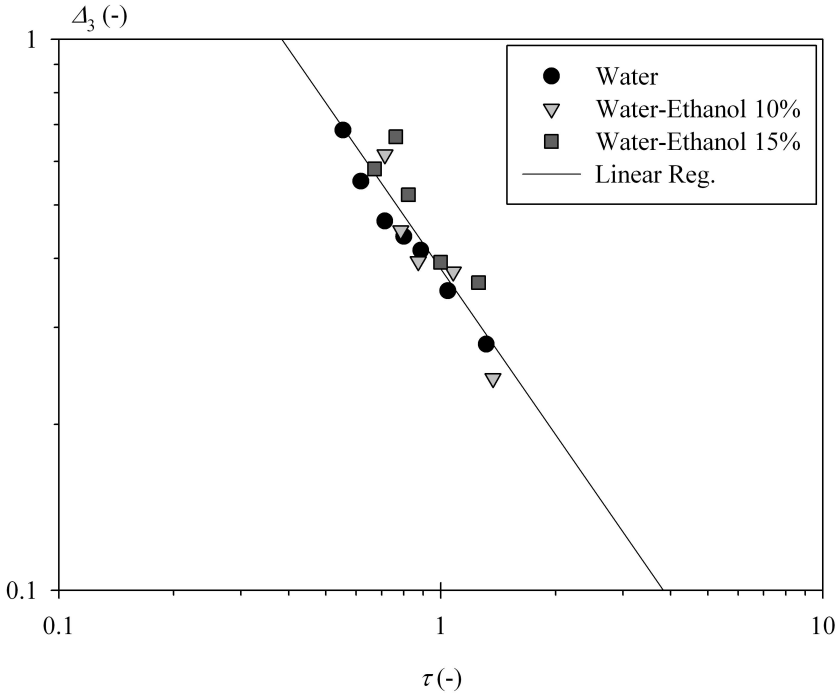


FIG. 7: Relative dispersion Δ_3 versus the number τ (all operating conditions).

shown in the literature, these distributions have no reason to be the same. This comparison is performed on the surface-based equivalent-diameter distributions. As stated in the previous section, IAT reports such a distribution. As far as the LDT is concerned, the surface-based equivalent-diameter distribution $f_2(D)$ is deduced from the measured volume-based distribution $f_3(D)$ by

$$f_2(D) = \frac{D_{32}}{D} f_3(D) \quad (5)$$

Comparisons of surface-based diameter distributions are shown in Fig. 8 (water, two injection pressures). At $\Delta P_i = 0.4$ MPa, the IAT and LDT surface-based diameter distributions are very much alike, denoting a moderate influence of the drop shape on the equivalent-diameter distributions in this condition. The literature specifies that the LDT sensitivity to the shape is minimized for objects with aspect ratios up to two-to-one (Black et al., 1996). An elliptic object with such aspect ratio has a uniformity parameter equal to $\eta = 0.7$. At $\Delta P_i = 0.4$ MPa, there are drops with a uniformity parameter greater than 0.7. (The maximum η value in this case is greater than 2.) The result in Fig. 8 says that the number of such drops at 0.4 MPa is small enough to limit their influence on the LDT equivalent-diameter distribution. Note that both diagnostics report a fractal characteristic in the small diameter region that manifests by a linear behavior in a log-log

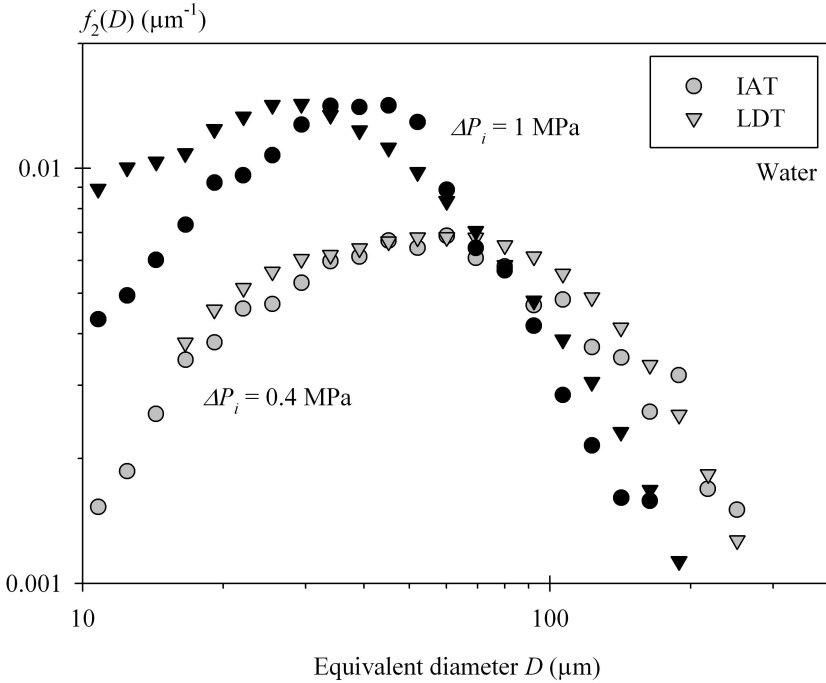


FIG. 8: Comparison of LDT and IAT surface-based diameter distributions (water, $\Delta P_i = 0.4$ MPa and 1.0 MPa).

coordinate system. Such characteristic has commonly been reported in LDT volume-based diameter distribution (Agüera et al., 2006; Dumouchel et al., 2012a). Note finally a slight left shift of the LDT distribution in the small diameter region.

For greater injection pressures (see the case $\Delta P_i = 1$ MPa in Fig. 8 for instance) the two diagnostics report different surface-based diameter distributions. The modal diameter of the LDT distribution is smaller than the one of the IAT distribution. A similar shift between LDT and IAT distributions was reported by Barreiros et al. (1996) when analyzing sets of nonspherical objects. The observations at 1 MPa in Fig. 8 are therefore likely due to the presence of nonspherical drops and to a different sensitivity of the diagnostics to drop shapes. Another agreement with Barreiros et al. (1996) can be noticed: the LDT equivalent diameter is not equal to the projected area diameter, the latter being measured by IAT.

The main difference is located in the small-diameter region where LDT distribution is greater than IAT distribution. Furthermore, the fractal characteristic of the LDT distribution is less than the one of the IAT distribution. The IAT distribution in the small-diameter region is believed to correspond to the *actual* small-drop population (see the previous section). Therefore, since the difference between LDT and IAT distributions is attributable to the shape of the drops, Fig. 8 suggests that the drop shape has an

influence on the LDT small-drop population. In particular, the deviation from sphericity of medium and large drops seems to impose a LDT fractal characteristic in the small-diameter region smaller than the one of the *actual* small-drop population.

The LDT fractal characteristics estimated in the diameter range [10 μm ; 17 μm] are presented in Fig. 9 for every working condition as a function of τ . Generally speaking, we note a decrease of the LDT fractal characteristic as τ decreases, that is, according to Fig. 5, when the spray drops are more and more deformed in average. (Some points for high τ numbers in Fig. 9 escape from this behavior, but, for these cases, we must mention that small-diameter classes are not very populated and lead to low accurate fractal characteristics.) This behavior supports the idea that the LDT fractal characteristic depends on the shape of the drops. In the following section, the LDT distributions are modeled in order to demonstrate the relationship between the LDT small-drop population and the shape of *actual* medium and large drops.

3.2 Modeling of the LDT Drop Size Distribution

The model consists of representing the LDT equivalent-diameter volume-based distribution by the three-parameter Generalized Gamma (3pGG) function, which is another form of the well-known Nukiyama–Tanasawa distribution. The 3pGG function is defined by

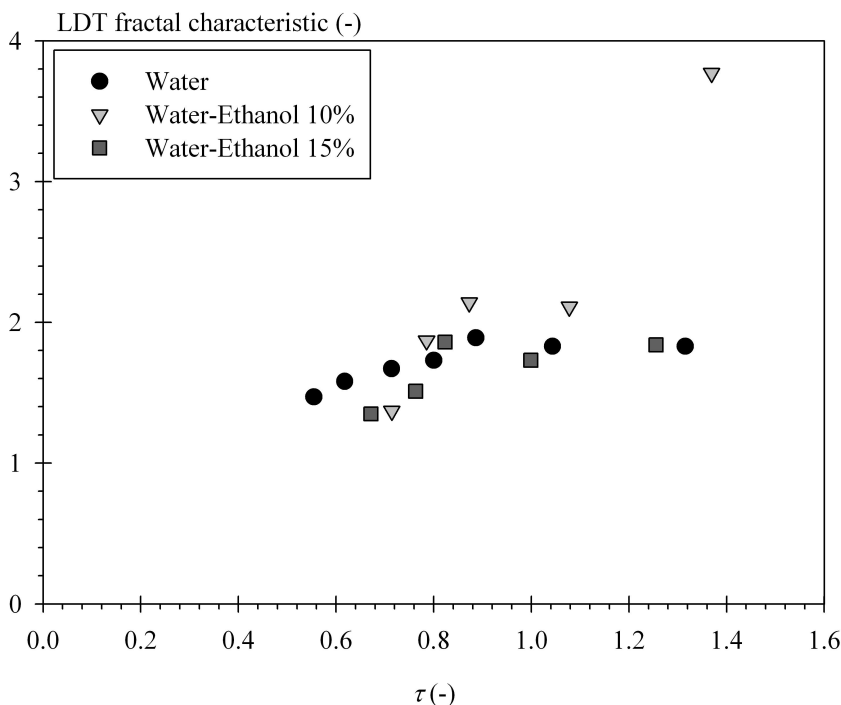


FIG. 9: LDT fractal characteristic versus the number τ .

$$f_n(D) = \frac{q}{\Gamma((\alpha+n)/q)} \left(\frac{\alpha}{q}\right)^{(\alpha+n)/q} \frac{D^{\alpha+n-1}}{D_{q0}^{\alpha+n}} \exp\left(-\frac{\alpha}{q} \left(\frac{D}{D_{q0}}\right)^q\right) \quad n = 0, 1, 2, 3 \quad (6)$$

where Γ is the Gamma function. The four types of distribution designated by $n = 0, 1, 2,$ or 3 correspond to the number-based, length-based, surface-based or volume-based diameter distribution. The three parameters are q and α , which both are dispersion parameters with no dimension, and the size parameter D_{q0} . Characteristics of the distribution can be expressed as a function of the three parameters. For instance, the expression of the traditional mean-diameter series D_{kl} and of the relative dispersion Δ_n can be established:

$$\begin{cases} D_{kl} = \left(\frac{q}{\alpha}\right)^{(1/q)} \left(\frac{\Gamma((\alpha+k)/q)}{\Gamma((\alpha+l)/q)}\right)^{1/(k+1)} D_{q0} \\ \Delta_n = \frac{\Gamma((\alpha+n)/q) \Gamma((\alpha+n+2)/q)}{\Gamma^2((\alpha+n+1)/q)} - 1 \end{cases} \quad (7)$$

It has been shown (Dumouchel et al. 2012a) that when q and α are chosen positive (which corresponds to the choice made in the present analysis) and if $q > 1$, the fractal characteristic in the small-diameter region of the 3pGG function depends on the parameter α and on the distribution order n only, i.e.,

$$f_n(D) \propto D^{\alpha+n-1} \text{ when } D \rightarrow 0 \quad (8)$$

Otherwise, i.e., when $q < 1$, the fractal characteristic of the 3pGG function becomes dependent on q also: it decreases as q decreases. In accordance with this property, the shape of the 3pGG function and its fractal characteristic in the small-diameter region are independent characteristics. For this reason, the 3pGG function was found very competent to reproduce LDT information including the volume-based equivalent-diameter distribution shape, the fractal characteristic in the small-diameter region, and the mean-diameter series (Dumouchel et al., 2012a). To obtain results of such a quality, a protocol to determine the parameters of the mathematical distribution was elaborated. This protocol is applied in the present work. It counts two steps:

1. The parameter α is determined from the fractal characteristic of the *actual* small-drop population, i.e., the one measured by IAT. According to Eq. (8), the parameter α is obtained from

$$f_2(D) \propto D^{\alpha+1} \quad (9)$$

where $f_2(D)$ is the surface-based equivalent-diameter distribution reported by IAT. It is important to remember that according to the results shown in Fig. 8, the fractal characteristics of IAT and LDT distributions are generally not equal. Thus, Eq. (9) does not apply for the surface-based diameter distribution of the LDT equivalent system of spherical drops.

2. The parameters q and D_{q0} are determined in order that the 3pGG function [Eq. (6)] best fits the LDT volume-based equivalent-diameter distribution. This is achieved by determining the couple (q, D_{q0}) that minimizes the sum S defined by

$$S = \sum_{i=1}^N \left(f_3^{\text{LDT}}(D_i) - f_3^{\text{3pGG}}(D_i) \right)^2 \quad (10)$$

where N is the number of diameter classes, D_i the class median diameter series, and f_3^{LDT} and f_3^{3pGG} designate the LDT and 3pGG volume-based equivalent-diameter distribution, respectively. The minimization of S is performed with the software Scilab.

The parameters α obtained from the IAT distribution according to step 1 are presented in Fig. 10 as a function of the Reynolds number of the flow issuing from the nozzle. The results organize as a single linear relationship denoting a strong influence of the turbulent level of the flow issuing from the nozzle on the dispersion in the small-diameter region. This result appears relevant for an atomization process that is known to depend on the initial turbulent level and to be free of aerodynamic effects (Dumouchel et al., 2005). We note in Fig. 10 that the correlation is rather independent of the liquid physical properties. Keep in mind that the dispersion in the small-diameter region does

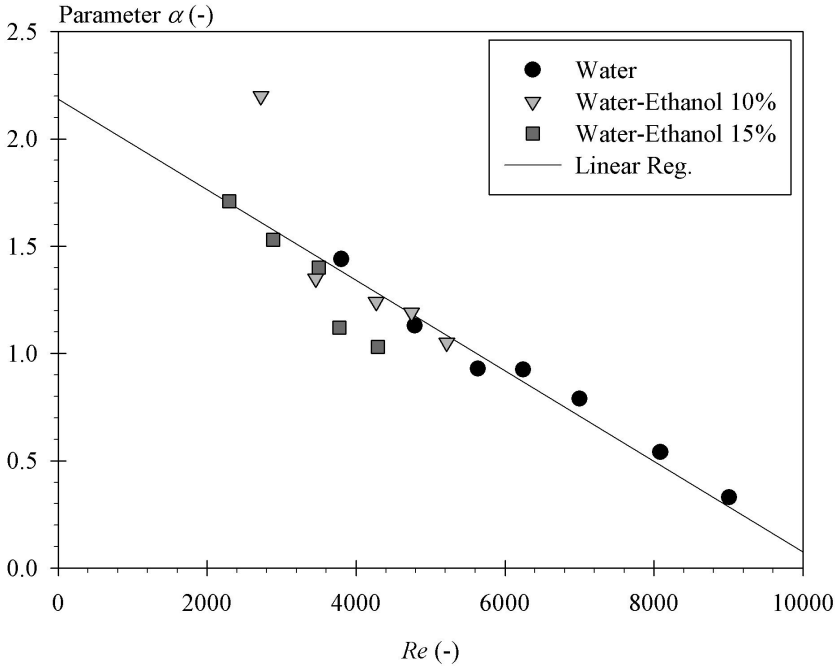


FIG. 10: Parameter α versus the Reynolds number.

not inform on the drop diameter distribution but on the spread of this characteristic in the small-diameter region.

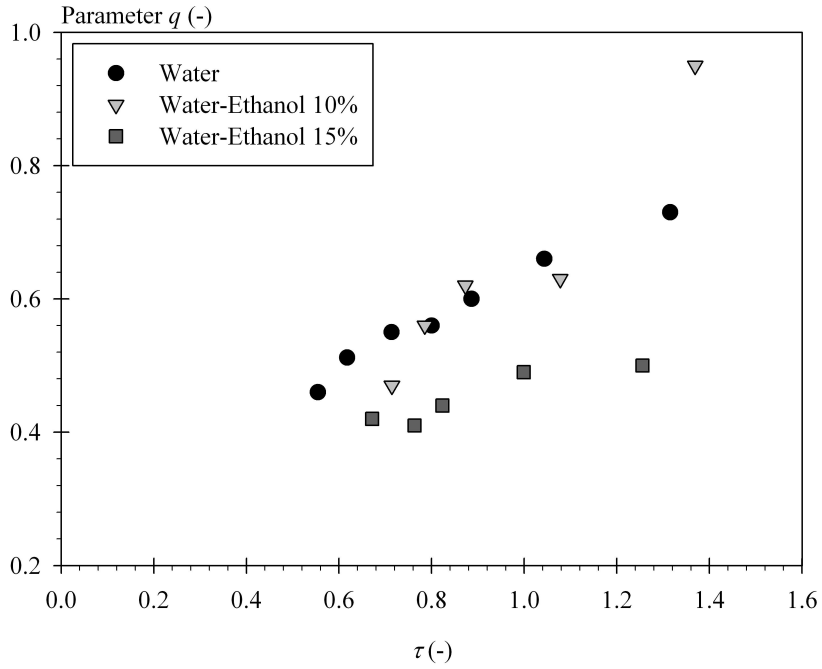
The values of the two other parameters obtained from step 2 are shown in Fig. 11 as a function of the number τ . Globally, the parameter q increases with τ [Fig. 11(a)] in a way that depends on the liquid properties. In Fig. 11(b), the parameter D_{q0} appears strongly related to the number τ in a way that is not influenced by the liquid physical properties.

The mathematical parameters found here (Figs. 10 and 11) show clear evolutions and are free of any stability problem, i.e., they do not vary drastically while the working conditions reasonably vary. This behavior comes from the fact that the parameter determination protocol is not based on a curve-fitting exercise only but incorporates physical information, i.e., the *actual* small-diameter dispersion (Dumouchel et al., 2012a). The quality of this modeling procedure is illustrated in Figs. 12 to 14. Figure 12 compares experimental and mathematical volume-based distributions for water. (The dots represent the measured LDT distribution and the lines the corresponding 3pGG function.) The agreement is very good. The same quality is obtained for the other working conditions. The relative dispersion Δ_3 of the experimental and mathematical distributions are compared with each other in Fig. 13. The mathematical relative dispersion Δ_3 shown in this figure are calculated with Eq. (7). As for the volume-based diameter distribution, we note that the agreement between the model and the experiment is very good.

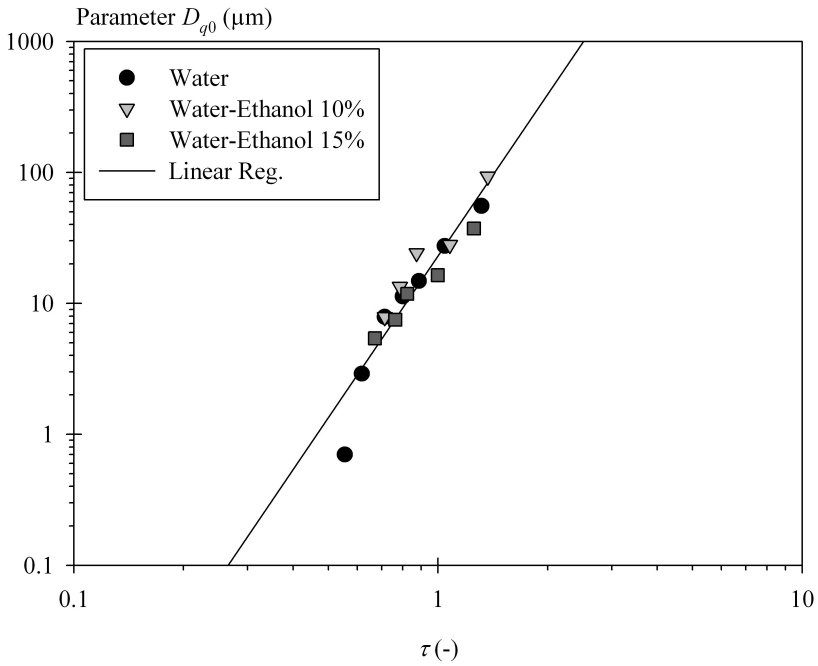
Finally, Fig. 14 shows that the fractal characteristics in the small-diameter region of the experimental LDT and mathematical 3pGG distributions are of the same order of magnitude. (The points that deviate most from this agreement are those for which the experimental fractal characteristic lacks accuracy.) We will see in the next section that this performance results from an advantageous adjustment of the dispersion parameter q . As far as the fractal characteristic is concerned, we see in Fig. 15 that the mathematical 3pGG function reports a single dependence with the number τ that homogenizes all working conditions. Supplementary work standing out of the focus of this work is required to establish the physical relevance of this behavior.

3.3 Interpretation and Discussion

The objective of the modeling presented in the previous section is to attest to the fact that the LDT distribution in the small-diameter region depends both on the *actual* small-drop population and on the shape of bigger drops. We see in Fig. 11(a) that the values of the parameter q are less than 1. As said above, this reveals that the fractal characteristics of the mathematical distributions and, therefore, those of the LDT diameter distributions, depend on both dispersion parameters, α and q . Determined from Eq. (9), the dispersion parameter α is representative of the *actual* small-drop population and is by no mean related to the shape of the drops. Thus, the question of the possible correlation between the parameter q and the shape of the drops arises. By plotting the average shape parameters



(a)



(b)

FIG. 11: Parameters q (a) and D_{q0} (b) versus the number τ .

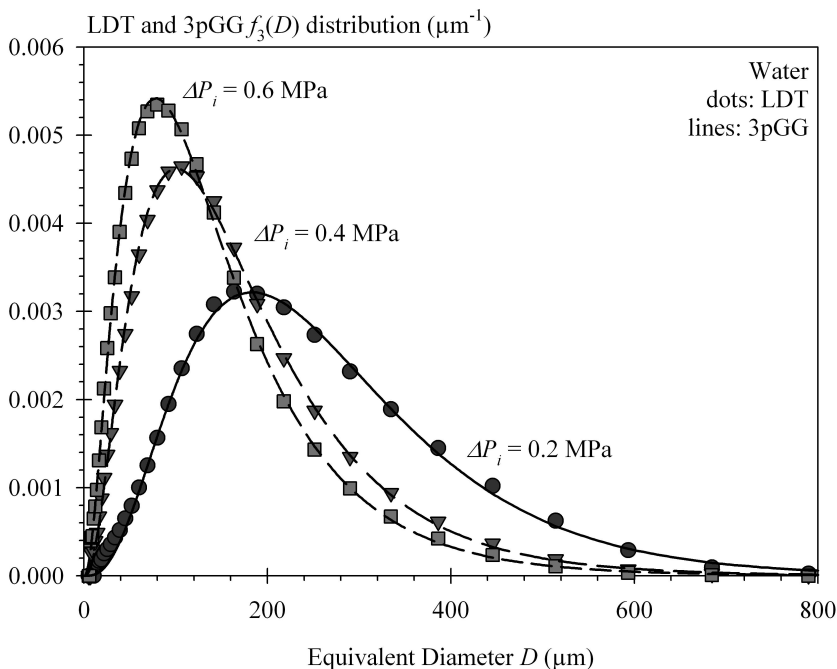


FIG. 12: Comparison between LDT and 3pGG diameter distributions.

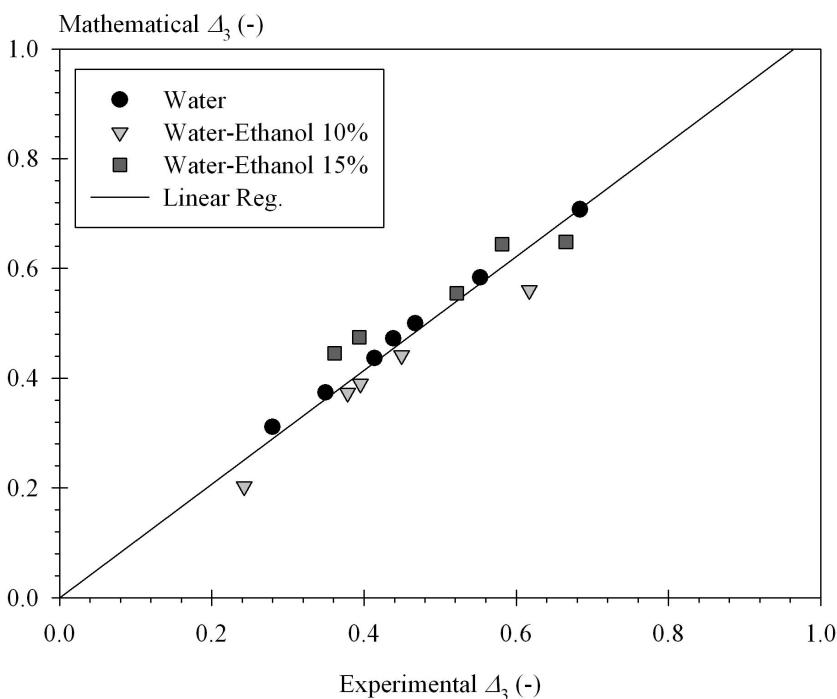


FIG. 13: Comparison between experimental and mathematical relative dispersion.

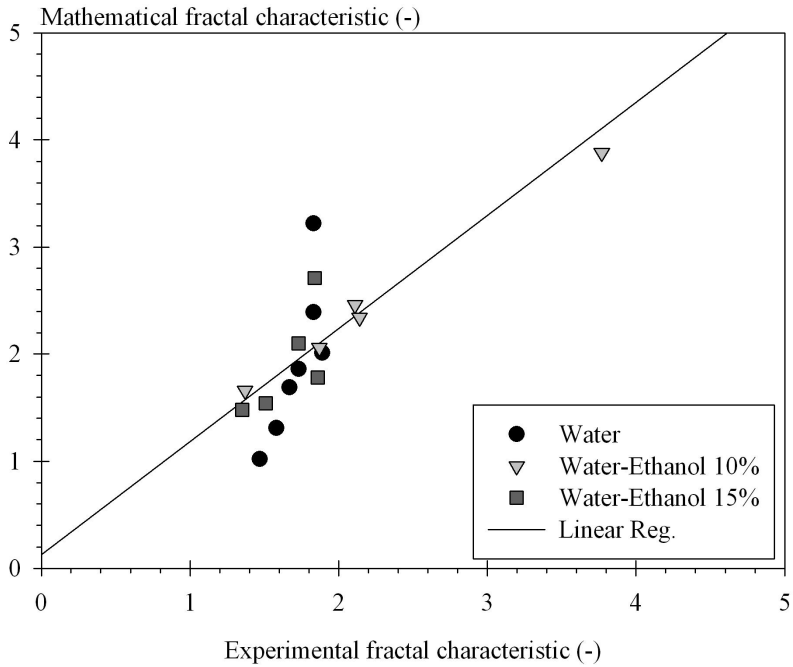


FIG. 14: Comparison between experimental and mathematical fractal characteristics.

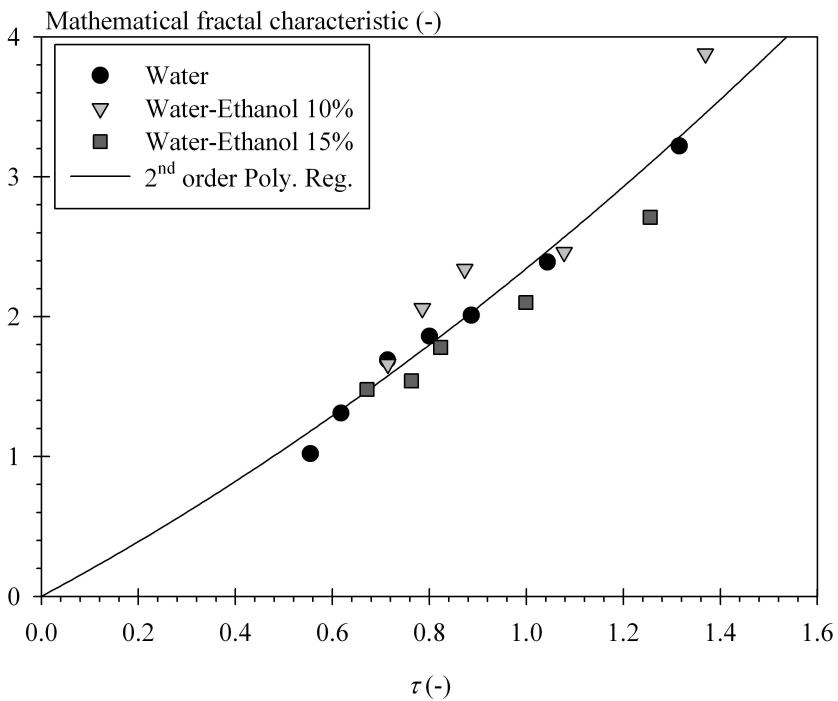


FIG. 15: Mathematical fractal characteristic versus the number τ .

as a function of the parameter q for all situations, Fig. 16 gives a clear answer to this question. We see that the parameter q strongly correlates with the average shape parameters: it decreases when the shape parameters increase. As explained above, a decrease of the parameter q in this condition induces a decrease of the fractal characteristic of the distribution in the small-diameter region. In consequence, the small-drop population of the LDT equivalent system is overestimated compared to the *actual* small-drop population when medium and large drops conspicuously deviate from sphericity. This suggests that LDT analyzes nonspherical drops as clusters of small drops.

Figure 16 confirms that a LDT distribution parameter q greater than 1 characterizes sets of spherical droplets. In this configuration, the LDT distribution fractal characteristic should be equal to the one of the *actual* small-drop population. The measurement performed with the reticle and shown in Fig. 2 is a conclusive illustration of this point.

This analysis demonstrates that, besides a natural dependence with the *actual* small-drop population, the dispersion in the small-diameter region of the set of spherical drops represented by the LDT equivalent-diameter volume-based distribution depends on the shape of the drops. Two points of discussion can be added.

The dispersion in the large-diameter region is also very much dependent on the parameter q . When q decreases, the dispersion in this region increases. This manifests by

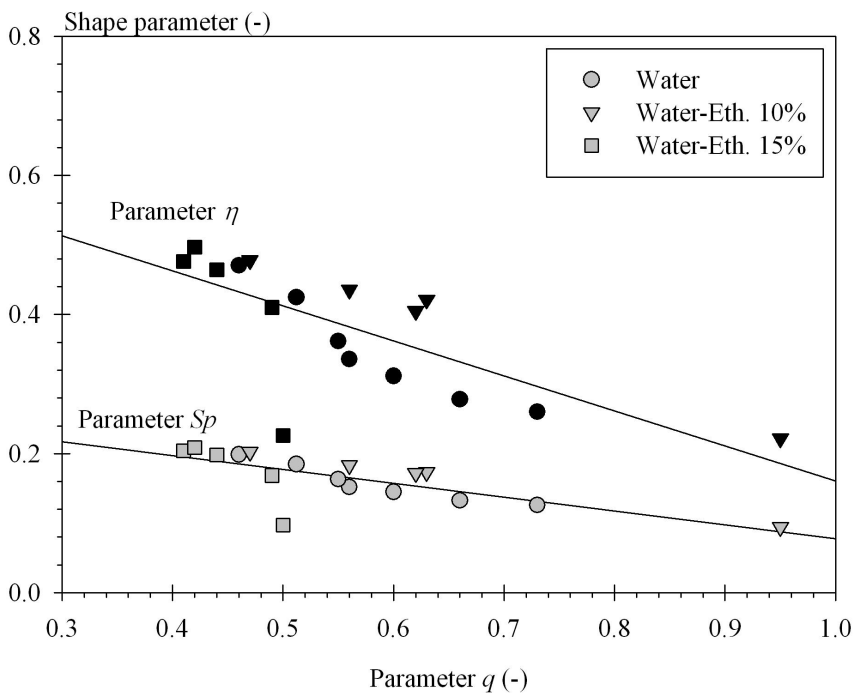


FIG. 16: Relationship between the shape parameters and the parameter q .

an extended tail toward the large-diameter region. Thus, the set of spherical drops represented by the LDT equivalent-diameter volume-based distribution has extended dispersions on both sides of the distribution. A numerical investigation due to Mühlenweg and Hirleman (1998) reproducing LDT measurements on sets of elliptic particles reported the same behavior.

Furthermore, the increase of dispersion in the large-diameter region of the LDT distribution resulting from the presence of nonspherical drops has an influence on the mean-diameter series. Figure 17 shows examples of mean-diameter ratio D_{m2}/D_{32} as a function of the order m . We see that the dependence between the mean diameters and the order m is a function of the injection pressure: the correlation evolves from a linear relationship to a second-order relationship when the injection pressure increases, i.e., when the *actual* drops are less and less spherical in average. Such relationships agree with those reported in a previous work (Dumouchel et al., 2010). Thus, the mean-diameter series of the set of spherical drops represented by the LDT distribution is sensitive to the shape of the drops. Note that such behavior has been evoked by others (Endoh et al., 1998; Dumouchel et al., 2010). Note also in Fig. 17, the mathematical mean-diameter

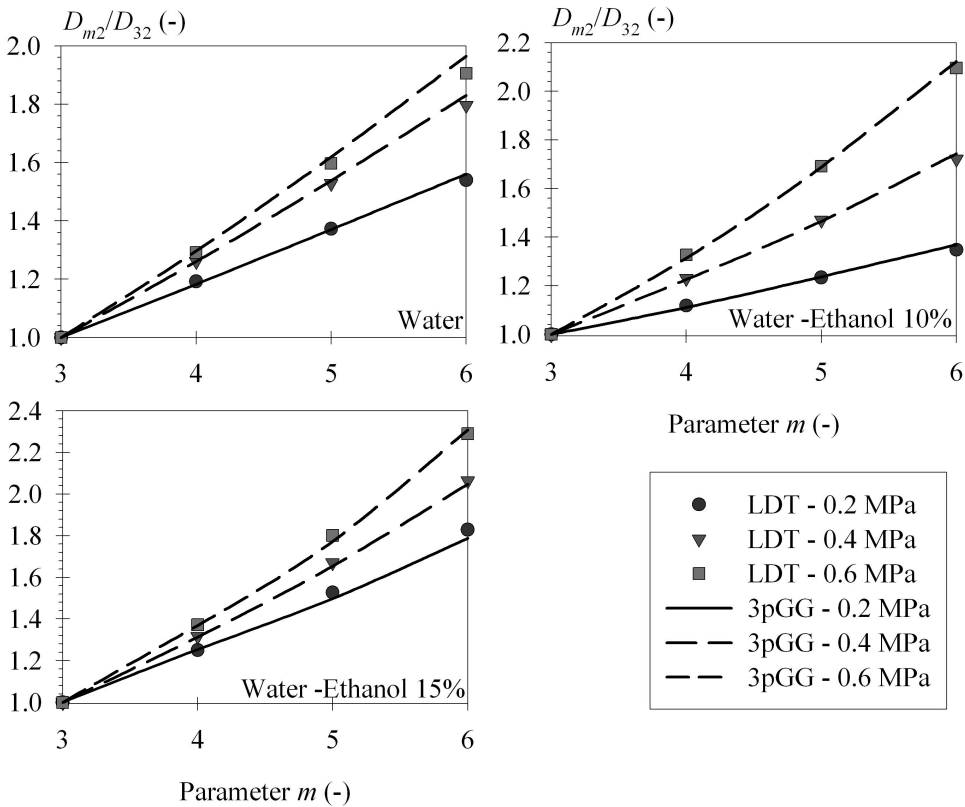


FIG. 17: Comparison of the experimental and mathematical mean-diameter series.

series satisfactorily agree with those experimentally obtained. This result is another evidence of the appropriateness of the 3pGG function to represent LDT distributions.

Finally, results obtained in a previous investigation suggested that the set of spherical drops represented by the LDT distribution has the same surface-based scale distribution as the *actual* set of drops (Dumouchel et al., 2010). The results found here reveal that this cannot be true. In particular, the extension of the dispersion in the large-diameter region because of nonspherical drops indicates that the maximum scale of the set of spherical drops represented by the LDT distribution is greater than the maximum scale of the *actual* system. To illustrate this, the surface-based scale distribution of the *actual* spray has been measured from IAT and compared with the LDT equivalent system surface-based scale distribution that is obtained from the relation

$$e_2(D_s) = \frac{2}{D_{q0}} \left(\frac{\alpha}{q} \right)^{1/q} \frac{\Gamma((\alpha + 1)/q, X_s) - X_s^{1/q} \Gamma(\alpha/q, X_s)}{\Gamma((\alpha + 2)/q)} \quad (11)$$

where $X_s = \frac{\alpha}{q} \left(\frac{D_s}{D_{q0}} \right)^q$

(For details concerning the definition and the measurement of surface-based scale distribution $e_2(D_s)$ from IAT, refer to Dumouchel et al., 2010.) Figure 18 shows a comparison

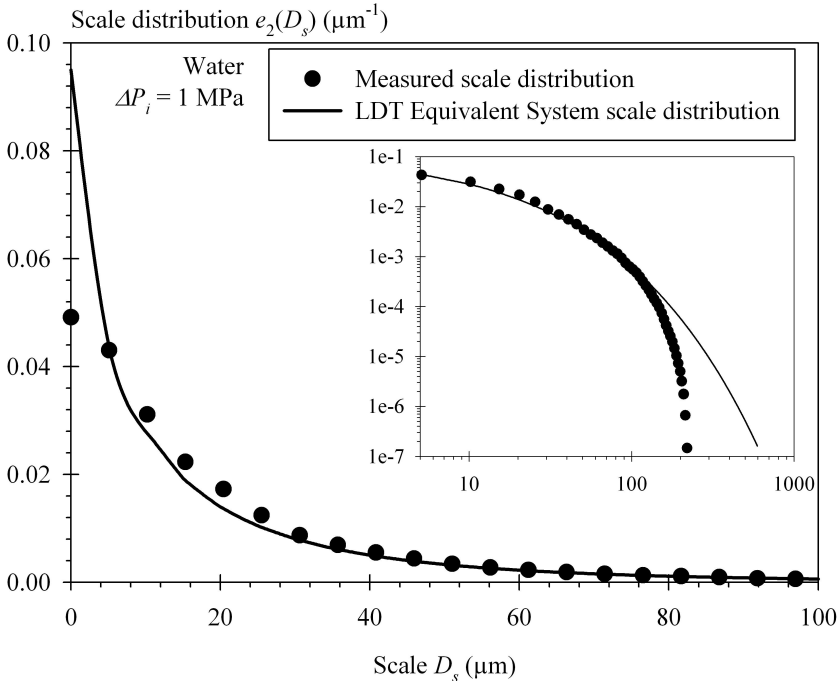


FIG. 18: Comparison of the scale distributions of the *actual* system and of the LDT equivalent system.

for water at $\Delta P_i = 1$ MPa. Provided in a linear coordinate system as well as in a log–log coordinate system, this comparison highlights that the set of spherical drops represented by the LDT distribution reports greater scale-distribution values in the small and large scale ranges. In the medium scale range, the difference is inverted. The equality between the LDT equivalent system and the *actual* system surface-based scale-distributions obtained in Dumouchel et al. (2010) was because the drop shapes were close to sphericity. Indeed, the equality was noticed at low injection pressure only, for which, as found here, the drop deformation has a moderate influence on the LDT measurement.

4. CONCLUSIONS

The present work contributes to a better understanding of the volume-based diameter distribution reported by a laser diffraction technique (LDT) when probing sprays containing nonspherical drops. Being controlled by the jump of pressure at the interface, the shape of a drop is related to its size and velocity. Globally speaking, small drops are spherical, and the deviation from sphericity increases with the size or/and the velocity of the drops. When probing a spray containing nonspherical drops, the LDT reports a volume-based diameter distribution that represents the set of spherical drops that would produce the same forward light scattered pattern as the one recorded. It is found that the small-drop population of this equivalent system depends on the *actual* small-drop population as well as on the shape of the *actual* drops. This double dependence results in a smaller fractal characteristic in the small-diameter region of the equivalent system compared to this very characteristic of the *actual* spray. This suggests that LDT analyzes nonspherical drops as clusters of smaller drops. The dispersion of the equivalent system in the large-diameter region also depends on the shape of the *actual* drops: it extends as the drops deform more and more and modifies the correlation between the LDT mean diameters D_{m2} and their order m .

These results have been demonstrated by modeling the LDT distributions with a 3-parameter Generalized Gamma (3-pGG) function. This function appears very appropriate to reproduce the LDT diameter distribution including the distribution shape, fractal characteristic in the small-diameter range, the relative dispersion, and the mean diameter series. An important point is the total absence of mathematical parameter instability. This gives physical weight to the present mathematical parameters and pleads in favor of the determination protocol applied here. In this protocol, one of the dispersion parameter introduced by the 3pGG function characterizes the fractal characteristic in the small-diameter region of the *actual* spray. In the present work, this dispersion parameter is determined from the IAT distribution in the small-diameter region and correlates with the Reynolds of the liquid flow issuing from the nozzle. This, of course, is a characteristic of the present atomization process. The second dispersion parameter depends on the shape of the actual drops. The fractal characteristic in the small-diameter region of the LDT distribution depends on both dispersion parameters. The extension of the

dispersion in the large-diameter region of the LDT distribution is a function of the second dispersion parameter. These results suggest that quantitative information on the drop shape might be obtained from the LDT distribution provided that the second dispersion parameter can be obtained from this distribution without resorting to another diagnostic. Although more work is required to conclude on this very point, this work suggests focusing this research on the mean diameter series.

REFERENCES

- Agüera, F., Aguilar, F. J., Aguilar, M. A., and Carvajal, F., Atomization characteristics of hydraulic nozzles using fractal geometry, *Trans. Am. Soc. Agric. Biol. Eng.*, vol. **49**, pp. 581–587, 2006.
- Barreiros, F. M., Ferreira, P. J., and Figueiredo, M. M., Calculating shape factors from particle sizing data, *Part. Part. Syst. Charact.*, vol. **13**, pp. 368–373, 1996.
- Black, D. L. and McQuay, M. Q., Laser-based particle measurements of spherical and nonspherical particles, *Int. J. Multiphase Flow*, vol. **27**, pp. 1333–1362, 2001.
- Black, D. L., Queiroz McQuay, M. and Bonin, M. P., Laser-based techniques for particle-size measurement: A review of sizing methods and their industrial applications, *Prog. Energy Combust. Sci.*, vol. **22**, pp. 267–306, 1996.
- Blaisot, J. B. and Yon, J., Droplet size and morphology characterization for dense sprays by image processing: Application to the diesel sprays, *Exp. Fluids*, vol. **39**, pp. 977–994, 2005.
- Dumouchel, C., Blaisot, J. B., and Dung, V. D., On the adequacy between the laser diffraction distribution and the 3-parameter Generalized Gamma function, *Chem. Eng. Sci.*, vol. **79**, pp. 103–111, 2012a.
- Dumouchel, C., Blaisot, J. B., and Dung, V. D., Representation of Laser Diffraction Diameter Distribution with a 3-Parameter Generalized-Gamma Function, in *Proc. Of 12th Intl. Conf. Liquid Atomization and Spray Systems*, Sept. 2–6, 2012, Heidelberg, Germany, 2012b.
- Dumouchel, C., Cousin, J., and Triballier, K., On the role of the liquid flow characteristics on low-Weber-number atomization processes, *Exp. Fluids*, vol. **38**, pp. 637–647, 2005.
- Dumouchel, C., Grout, S., Leroux, B., and Paubel, X., Experimental determination of liquid spray drop morphology qualitative information from laser-diffraction measurements, *Part. Part. Syst. Charact.*, vol. **27**, pp. 76–88, 2010.
- Endoh, S., Kuga, Y., Ohya, H., Ikeda, C., and Iwata, H., Shape estimation of anisometric particles using size measurement techniques, *Part. Part. Syst. Charact.*, vol. **15**, pp. 145–149, 1998.
- Fdida, N. and Blaisot, J. B., Drop size distribution measured by imaging: Determination of the measurement volume by the calibration of the point spread function, *Meas. Sci. Technol.*, vol. **21**, pp. 1–15, 2010.
- Ghaemi, S., Rahimi, P., and Nobes, D. S., Assessment of parameters for distinguishing droplet shape in a spray field using image-based techniques, *Atomization Sprays*, vol. **19**, pp. 809–831, 2009.
- Guardiani, R., Nascimento, C. A. O., and Onimaru, R. S., Use of neural networks in the analysis

- of particle size distribution by laser diffraction: Tests with different particle systems, *Powder Technol.*, vol. **126**, pp. 42–50, 2002.
- Loth, E., Quasi-steady shape and drag of deformable bubbles and drops, *Int. J. Multiphase Flow*, vol. **34**, pp. 523–546, 2008.
- Mülhenweg, H. and Hirleman, E. D., Laser diffraction spectroscopy: Influence of particle shape and a shape adaptation technique, *Part. Part. Syst. Charact.*, vol. **15**, pp. 163–169, 1998.
- Sowa, W. A., Interpreting mean drop diameters using distribution moments, *Atomization Sprays*, vol. **2**, pp. 1–15, 1992.